Published in final edited form as:
J Phys Chem A. 2002 June 27; 106(25): 6030–6038.

Vibrational Relaxation in β-Carotene Probed by Picosecond Stokes and Anti-Stokes Resonance Raman Spectroscopy

David W. McCamant, **Judy E. Kim**, and **Richard A. Mathies***
Department of Chemistry, University of California, Berkeley, California 94720

Abstract

Picosecond time-resolved Stokes and anti-Stokes resonance Raman spectra of *all-trans*-β-carotene are obtained and analyzed to reveal the dynamics of excited-state (S_1) population and decay, as well as ground-state vibrational relaxation. Time-resolved Stokes spectra show that the ground state recovers with a 12.6 ps time constant, in agreement with the observed decay of the unique S_1 Stokes bands. The anti-Stokes spectra exhibit no peaks attributable to the S_1 ($2A_g^-$) state, indicating that vibrational relaxation in S_1 must be nearly complete within 2 ps. After photoexcitation there is a large increase in anti-Stokes scattering from ground-state modes that are vibrationally excited through internal conversion. The anti-Stokes data are fit to a kinetic scheme in which the C=C mode relaxes in 0.7 ps, the C–C mode relaxes in 5.4 ps and the C–CH_3 mode relaxes in 12.1 ps. These results are consistent with a model for S_1–S_0 internal conversion in which the C=C mode is the primary acceptor, the C–C mode is a minor acceptor, and the C–CH_3 mode is excited via intramolecular vibrational energy redistribution.

Introduction

The electronic structure and photodynamics of carotenoids are of interest because carotenoids play important roles as light-harvesting and photoprotective agents in photosynthetic systems.[1] The visible absorption band in carotenoids is due to the $1A_g^-$ (S_0) → $1B_u^+$ (S_2) transition. In general, the S_2 state relaxes to the S_1 ($2A_g^-$) state on the subpicosecond time-scale in all carotenoids, but the S_1–S_0 relaxation rate is slower and depends on the conjugation length.[2] The time-scale for S_1 → S_0 relaxation ranges from ~0.5 ps for long carotenoids with 19 conjugated C=C bonds, to ~300 ps for short carotenoids with 7 conjugated C=C bonds.[3,4] In β-carotene, S_2 to S_1 internal conversion (IC) occurs in ~200 fs[5-9] and internal conversion from S_1 to S_0 occurs in ~8–10 ps.[5,10,11] Both IC rates follow the energy gap law formulated using an adiabatic weak-coupling model.[12] Recently, however, conical intersections have been discovered in shorter polyenes and implicated in both IC processes.[13,14] The conical-intersection model of IC reproduces the same energy gap dependence but invokes dynamic relaxation and strong coupling between the electronic states at the conical intersection.

In photosynthetic systems, the ability of a carotenoid to transfer excitation to nearby chlorophylls is determined by the relative energies of the carotenoid S_1 state and the chlorophyll Q_y state. To explore these energetics, the rate of intramolecular vibrational energy redistribution (IVR) and vibrational cooling in the S_1 state of carotenoids has been extensively investigated.[4,15-18] Two of these studies suggested that vibrational relaxation in S_1 occurs more slowly than IC. Zhang et al.[15] assigned several features in the S_1 absorption band of lycopene to vibrational hot-bands and found that these bands did not decay faster than the other bands in the spectrum. However, their time-resolution was limited to ~3 ps, which is longer than the usual time-scale for excited-state IVR.[19] Yoshizawa et al.[16] suggested that β-carotene relaxed

*To whom correspondence should be addressed. E-mail: rich@zinc.cchem.berkeley.edu. Phone: (510) 642-4192. Fax: (510) 642-3599.

in 600 fs to the $v = 1$ (C=C) state but that relaxation to $v = 0$ proceeded more slowly than IC. However, their conclusions depended on a complicated interpretation involving competing stimulated and inverse Raman effects and a 40 cm^{-1} anharmonic shift in the S_1 C=C frequency. These conclusions are inconsistent with femtosecond transient absorption studies of β-carotene,[17] spheroidene,[18] and long-chain carotenoids,[4] which found that IVR and vibrational cooling in S_1 occur in <1 ps. It is evident that a more complete understanding of IVR and vibrational cooling in the S_1 states of carotenoids is needed.

Previous time-resolved anti-Stokes Raman experiments on carotenoids have observed the expected increase in S_0 anti-Stokes signals after photoexcitation to S_2 and subsequent IC. The anti-Stokes signal from spirilloxanthin grew in by ~3 ps, closely matching the S_1–S_0 IC time constant, and decayed with a ~10–15 ps cooling time.[20,21] In a related study of canthaxanthin, the anti-Stokes rise-time fit the known S_1–S_0 IC time constant and the signal decayed with a 15–20 ps time constant.[22] Additionally, it was shown that at 6 ps, the signal arose from molecules in low ($v = 1$ or 2) vibrational states, indicating that IVR must have occurred in <6 ps. However, these studies did not observe any S_1 features or kinetics that would report on excited-state IVR processes.

Here, we have performed simultaneous Stokes and anti-Stokes time-resolved Raman experiments on β-carotene in order to elucidate the time-scales of vibrational relaxation in both the S_1 and S_0 states. Our results show that S_1 vibrationally relaxes in <2 ps, much faster than the S_1–S_0 internal conversion time, and that IVR and vibrational cooling in the ground state occur over a range of times (1–12 ps) suggesting mode-specific cooling rates in S_0.

Materials and Methods

all-trans-β-Carotene (Aldrich) was recrystallized from benzene and methanol. An ~18 μM solution of β-carotene (λ_{max} = 463 nm, OD_{463} = 0.247 mm^{-1}, ε_{max} = 139 000 M^{-1} cm^{-1}) in toluene was prepared from dried crystals under dim light and stored under nitrogen. The sample was kept on ice and circulated through a 2 mm square cell in a closed loop under nitrogen. The flow rate of the solution (200 μm/ms) was chosen so that the illuminated sample volume was completely replaced between shots. The OD at the pump wavelength was 0.075 mm^{-1} and the OD at the probe wavelength was 0.010 mm^{-1}. The absorption spectrum did not exhibit any observable changes over the course of the experiment.

Instrumentation

The picosecond resonance Raman laser system has been described in detail elsewhere.[23,24] Briefly, a picosecond Ti:Sapphire oscillator (Spectra-Physics Tsunami model 3950) seeds a Ti:Sapphire regenerative amplifier (Spectra-Physics Spitfire) that produces a 1 kHz, 3 ps pulse train. After frequency doubling in BBO, the resultant 403 nm beam is Raman-shifted in a 0.5 m pipe filled with 1000 psi D_2 to produce the 531.5 nm second Stokes probe beam, while the residual SHG beam is used as the pump. The pulse width of the probe was 1.5 ps (16 cm^{-1} fwhm) and the pump/probe cross-correlation was 4.1 ps with an approximately Gaussian shape. Deconvolution of the cross-correlation, assuming Gaussian pulse shapes, indicates that the pump pulse fwhm was 2.9 ps. The pump−probe time delay was calibrated with sum-frequency generation in BBO to within ±0.5 ps.

The pump and probe beams were focused onto the flowing sample with a 50 mm f.l. spherical lens, producing a 50 μm diameter focal point. The average pump power at the sample point was 420 μW (4.3×10^{16} photons/cm^2/pulse) and the probe power at the sample point was 190 μW (2.6×10^{16} photons/cm^2/pulse). With a 5 ps pump−probe delay, the growth in intensity of the S_1 Stokes peaks and S_0 anti-Stokes peaks and the decrease in intensity of the S_0 Stokes

peaks were linear in pump power from 350 to 550 μW. The changes in intensity of all Stokes and anti-Stokes peaks were linear in probe power from 150 to 260 μW.

Raman scattering was collected with an *f*/1.2, 50 mm f.l. camera lens and imaged onto the 200 μm (26 cm^{-1}) entrance slit of the spectrograph (Spex 500 M, 500 g/mm, 560 nm blaze) with an *f*/4, 200 mm f.l. singlet lens. The pump scattering was removed with a long-pass filter (Schott GG435), whereas the probe scattering was removed with a 1064.0 nm notch filter (Kaiser Optical) using its second-order blocking capability at 532 nm. The width of the optical notch was 10 nm, which allowed simultaneous collection of Stokes and anti-Stokes scattering to within 300 cm^{-1} of the probe wavelength. The dispersed light was detected with a liquid nitrogen cooled CCD (Princeton Instruments, LN/CCD-1100-PB/UVAR). The instrument response was determined with a tungsten standard lamp. Wavelength calibration was performed using a neon lamp. All absolute Raman shifts are accurate to ±4cm^{-1}, whereas relative shifts are accurate to ±0.5 cm^{-1}.

Pump + probe spectra were collected for 10 min at each pump + probe time delay, with probe-only and pump-only spectra measured for 5 min between each pump + probe time point. Spectra with twenty different time delays between −6 and 100 ps were acquired. The fluorescence background in the pump-only spectra exhibited no change over the approximately 12 h of data collection. Pump-only, probe-only, and pump + probe spectra of neat toluene were measured for 5 min each to provide solvent spectra.

Spectral Subtraction

Examples of corrected pump + probe, pump-only, and probe-only data are presented in Figure 1. In the pump + probe spectrum with Δt = 1 ps (solid line), the Raman lines of toluene and β-carotene are superimposed on the broad fluorescent background which is also evident in the pump-only spectrum (dashed). Comparing the Stokes Raman peaks of the pump + probe spectrum with the probe-only spectrum (dotted), the decreased relative intensity of the β-carotene peaks is visible, indicative of ground-state depletion by the pump pulse.

To visualize the pump-induced changes quantitatively, background-free time-resolved Raman spectra were generated from the pump + probe spectra using the subtraction procedure shown in Figure 2. The pump-induced fluorescence was removed by subtracting the pump-only spectrum (B) from the pump + probe spectra (A). The spectra were then corrected for self-absorption, using the toluene peaks as an internal standard, by dividing by the transmission spectrum ($T(\lambda)$) of a 1.4 mm effective path length β-carotene solution to produce spectrum C. This large effective path length indicates that the dynamic self-absorption occurring in the 50 μm illuminated spot has a negligible contribution relative to the static ground-state absorption. The toluene Raman peaks were then removed by subtracting the pure toluene probe-only spectrum (D), resulting in spectum E. Because of slight changes in the spectral profile of the probe beam over the course of the experiment, it was sometimes necessary to shift the toluene spectra slightly to obtain a proper solvent subtraction. The broad fluorescence background under the Stokes and anti-Stokes spectra was fit to a 19th order polynomial (F) and subtracted, leaving the background-free, time-resolved Raman spectrum of the ground and excited states of β-carotene (G). It was necessary to use a high-order polynomial to effectively fit the structure of the fluorescence over the broad spectral range of both the Stokes and anti-Stokes windows and to describe the decreased instrument response approaching the notch filter wavelength. A background-free Raman spectrum of S_0 β-carotene was obtained from the averaged probe-only spectra using the same spectral subtraction procedures as described above.

Kinetic Analysis

The kinetics of the Raman intensities were first analyzed by empirically fitting to the convolution of our Gaussian instrumental response with a single or double exponential molecular response

$$M(t) = A\cdot\left\{a_0\cdot\exp\left(\frac{-\left(t-\Delta t_0\right)}{\tau_0}\right)+a_1\cdot\exp\left(\frac{-\left(t-\Delta t_0\right)}{\tau_1}\right)\right\}+B \quad (1)$$

The functional form of eq 1 varied depending on the dynamics being considered. For the S_0 recovery, the parameters in eq 1 were chosen to produce an instantaneous bleach followed by a single-exponential recovery. For the S_1 peaks, the molecular response was set to a biexponential representing the fast formation and the slower decay of the S_1 population. The anti-Stokes signals were fit to a biexponential molecular response with different amplitudes for the two exponential terms allowing an instantaneous decrease in intensity followed by exponential rise above baseline and subsequent decay back to the baseline.

To more effectively analyze the anti-Stokes dynamics, it was necessary to develop a first-order kinetic model of the relaxation encompassing excitation from S_0 to S_2, fast relaxation from S_2 to S_1, internal conversion from S_1 to vibrationally hot S_0, and then cooling from hot S_0 to the final relaxed S_0 state. (Here, we use “hot” to refer to any molecular state that has excess vibrational energy relative to what would be expected for a Boltzmann population at 10 °C, the bulk sample temperature. We use “cooling” to refer to any process that reduces the excitation present in a particular vibrational mode. This cooling may occur by IVR or vibrational energy dissipation to the solvent.) Excitation creates an initial population in S_2 and relaxation of this population and subsequent time-dependent population changes in the other states can be solved exactly using first-order kinetics, assuming the relaxation scheme

$$S_0 \xrightarrow{h\nu} S_2 \xrightarrow{k_{21}=1/\tau_{21}} S_1 \xrightarrow{k_{10}=1/\tau_{10}} S_0^{hot} \xrightarrow{k_{00}=1/\tau_{00}} S_0 \quad (2)$$

where k_{21} and k_{10} are the $S_2 \rightarrow S_1$ and $S_1 \rightarrow S_0$ internal conversion rates, and k_{00} is the mode-specific cooling rate in S_0. With the conditions $\left[S_2(t)\right]+\left[S_1(t)\right]+\left[S_0^{hot}(t)\right]+\left[S_0(t)\right]=1$, $\left[S_0(0)\right]=1-\left[S_2(0)\right]$, and $\left[S_1(0)\right]=\left[S_0^{hot}(0)\right]=0$, the solutions to the time-dependent populations are as follows

$$\left[S_2(t)\right]=\left[S_2(0)\right]\cdot e^{-k_{21}t} \quad (3)$$

$$\left[S_1(t)\right]=\left[S_2(0)\right]\cdot\frac{k_{21}}{\left(k_{10}-k_{21}\right)}\cdot\left(e^{-k_{21}t}-e^{-k_{10}t}\right) \quad (4)$$

$$\left[S_0^{hot}(t)\right]=\left[S_2(0)\right]\cdot\left\{a_0\cdot e^{-k_{21}t}+a_1\cdot e^{-k_{10}t}+a_2\cdot e^{-k_{00}t}\right\} \quad (5)$$

$$\left[S_0(t)\right]=\left[S_0(0)\right]+\left[S_2(0)\right]\cdot\left\{1-\beta_0\cdot e^{-k_{21}t}-\beta_1\cdot e^{-k_{10}t}-\beta_2\cdot e^{-k_{00}t}\right\} \quad (6)$$

$$a_0 = k_{21}k_{10}/\left[\left(k_{10}-k_{21}\right)\left(k_{00}-k_{21}\right)\right],\ a_1 = k_{21}k_{10}/\left[\left(k_{21}-k_{10}\right)\left(k_{00}-k_{10}\right)\right],$$

Where $a_2=\beta_2=k_{21}k_{10}/\left[\left(k_{21}-k_{00}\right)\left(k_{10}-k_{00}\right)\right]$, $\beta_0=k_{10}k_{00}/\left[\left(k_{10}-k_{21}\right)\left(k_{00}-k_{21}\right)\right]$ and $\beta_1=k_{21}k_{00}/\left[\left(k_{21}-k_{10}\right)\left(k_{00}-k_{10}\right)\right]$

The net observed intensity of the S_0 Stokes and anti-Stokes peaks, relative to that observed in the probe-only spectrum, is

$$I(t)=\left[S_0(t)\right]+d\cdot\left[S_0^{hot}(t)\right] \quad (7)$$

where the S_0^{hot} coefficient, *d*, represents the relative increase or decrease in scattering from S_0^{hot} relative to the room-temperature S_0 population. The enhancement factor, *d*, parametrizes all contributions to the scattering intensity of the hot species including population and resonance enhancement changes. Because of the decrease in Stokes scattering cross-section with increasing temperature,[25] we might expect $d \leq 1$ for the Stokes peaks. However, this effect may be significantly attenuated by our use of a probe wavelength on the red edge of the absorption spectrum, where increased relative enhancement of vibrationally hot molecules is expected.[25] In the anti-Stokes spectrum, however, the increase in population in excited vibrational states in hot S_0 would increase anti-Stokes signal and therefore we would expect $d > 1$. Substituting eqs 5 and 6 into eq 7, we get

$$I(t) = 1 + \left[S_2(0)\right] \cdot \left\{ \left(d \cdot a_0 - \beta_0\right) e^{-k_{21} t} + \left(d a_1 - \beta_1\right) e^{-k_{10} t} + \left(d a_2 - \beta_2\right) e^{-k_{00} t} \right\} \quad (8)$$

The S_0 Stokes and anti-Stokes kinetics were fit to the convolution of eq 8 with the Gaussian instrumental response. In all of the fits, the zero of time was adjusted as discussed below. It should be noted that the only variable parameters in eq 8 are $[S_2(0)]$, *d*, k_{21}, k_{10}, and k_{00}; the α's and β's are functions of k_{21}, k_{10}, and k_{00} and are therefore not independent variables.

Results

Representative pump + probe spectra are presented in Figure 3 along with the probe-only spectrum. On both the Stokes and anti-Stokes sides of the probe-only spectrum, the three largest S_0 vibrational peaks are visible at 1004, 1157, and 1523 cm^{-1} corresponding to the methyl rock (C–CH_3), carbon single-bond stretch (C=C) and carbon double-bond stretch (C=C) normal modes.[26] Comparing the +2 and −2 ps pump + probe Stokes spectra, the decrease in intensity of the S_0 C–C and C–CH_3 peaks at 1157 and 1004 cm^{-1} is clearly visible. In addition, growth of the Stokes S_1 signal is evidenced by the broad shoulder that develops on the high-frequency side of the C=C band (~1230 cm^{-1}) and by the high-frequency C=C band (1781 cm^{-1}). The large increase in S_0 anti-Stokes scattering at positive time delays is due to the formation of hot S_0 molecules after internal conversion from S_2 through S_1 to S_0. Note also that no S_1 peaks are visible in the anti-Stokes spectra.

To clarify the positions and shapes of the S_1 and hot S_0 bands, the S_0 probe-only Stokes spectrum was subtracted from the pump + probe Stokes spectra until the S_0 peaks at 1004 and 1157 cm^{-1} were completely removed. The subtraction coefficient, $c(t)$, varied between 60 ± 2% at 6 ps and 101 ± 2% at 100 ps. A representative set of these Stokes difference spectra is presented in Figure 4. In the early difference spectra, the S_1 C–C band at 1230 cm^{-1}, the S_1 C=C peak at 1543 cm^{-1}, and the high-frequency S_1 C=C peak at 1781 cm^{-1} are observed. Although most of the S_0 peaks are removed by the subtraction, at longer time delays peaks from the hot ground state are visible on the low-frequency side of the S_0 C–C and C=C peaks at 1145 and 1509 cm^{-1}. These hot S_0 bands are not completely removed by the subtraction because they are anharmonically downshifted. Attempts to decompose the ~1200 and ~1530 cm^{-1} bands into separate S_1 and hot S_0 peaks were unsuccessful because of the complex shape and intensity evolution of the hot S_0 peaks.

Analysis of the kinetics of the Stokes spectra using eq 1 (see below) revealed that the decay-time, τ_0, was very sensitive to variations in the rise-time, τ_1, and the zero of time, Δt_0. It was thus necessary to adjust Δt_0 and to choose and fix the rise-time, τ_1, of the S_1 peaks. To determine τ_1, the S_1 peak kinetics (Figure 5c-e) were first fit using eq 1 and all parameters except a_0, a_1, and *B* were allowed to vary. The weighted mean of the best-fit values of τ_1 (0.2 ± 0.2 ps) was chosen and fixed in subsequent analyses that determined Δt_0 and τ_0. This value of τ_1 is consistent with the 144 ± 10 fs $S_2 \rightarrow S_1$ IC time constant determined in previous fluorescence

upconversion experiments in toluene.[9] To determine Δt_0, both the S_1 kinetics, with τ_1 fixed at 0.2 ps, and the S_0 recovery kinetics (Figure 5a,b) were fit. The weighted mean of all five fits gave $\Delta t_0 = 0.3 \pm 0.1$ ps, and this zero of time was used in all subsequent analyses.

The dynamics of ground state bleaching and recovery are revealed by the kinetics of the probe-only subtraction coefficients, $c(t)$ in Figure 5a, as well as the Stokes S_0 C–CH_3 intensity in Figure 5b. Although the bleaching of the ground state is also visible in the S_0 C–C and C=C Stokes peaks, the overlap of these features with S_1 bands dictates that their integrated areas are not strictly proportional to S_0 population. The $c(t)$ and the C–CH_3 kinetics were fit by a single-exponential molecular response using eq 1 with the best-fit parameters of $A = 56\%$, $\tau_0 = 12.0 \pm 0.7$ ps, and $A = 59\%$, $\tau_0 = 10.2 \pm 2.3$ ps, respectively. The weighted mean of these two amplitudes indicates that each pump pulse excited 56 ± 2% of the β-carotene in the illuminated sample. The kinetic model fits of the S_0 Stokes data using eq 8 gave poorer fits than the single-exponential molecular response. This is most likely because the Stokes scattering cross-section of hot S_0 is nearly the same as cool S_0 at our probe wavelength, making $d \approx 1$ in eqs 7 and 8 and the observed dynamics essentially independent of the cooling rate.

The analysis of the kinetics of the 1781 cm^{-1} C=C, 1543 cm^{-1} C=C, and ~1230 cm^{-1} C–C peaks of the S_1 excited state is presented in Figure 5c-e. As described previously, the rise time of the S_1 peaks was fixed at 0.2 ps. With this constraint, the decay times were determined to be 12.6 ± 1.3, 15.1 ± 1.2, and 13.2 ± 1.8 ps for the 1781, 1543, and 1230 cm^{-1} peaks respectively (see Table 1). Because the C=C peak at 1781 cm^{-1} is unencumbered by any overlap with S_0 peaks, it provides the best measure of the $S_1 \rightarrow S_0$ kinetics and indicates that this IC time constant is 12.6 ps. However, the fact that the decay time constants of the other Stokes kinetics in Figure 5 agree with this value within the error limits indicates that the contribution of hot S_0 scattering to the 1543 and 1230 cm^{-1} S_1 kinetics does not significantly perturb the results (see discussion below).

The normalized intensities of the S_0 anti-Stokes bands are presented in Figure 6. The S_0 anti-Stokes signal is expected to decrease instantaneously due to ground state depletion, to then increase above the probe-only level due to the formation of vibrationally excited molecules after internal conversion from S_1, and finally to decay back to the probe-only level via vibrational cooling. This is the observed behavior, although the initial decrease is only suggested in the C–CH_3 anti-Stokes data. Attempts to fit the anti-Stokes kinetics to a biexponential molecular response function (eq 1) were hampered by large uncertainty in the parameters. For completeness, however, these results are reported in Table 1 and Figure 6 (dotted). These fits indicated that the decay times of the C=C, C–C, and C–CH_3 peaks were 11.7 ± 2.6, 15.3 ± 3.7, and 16 ± 11 ps, respectively. The respective rise times of the peaks were 1.4 ± 0.7, 3.1 ± 1.4, and 6.8 ± 5.5 ps.

A more precise analysis of the anti-Stokes kinetics was obtained by fitting the anti-Stokes data to the convolution of our instrument response with the kinetic model described by eq 8. The results of these fits are shown in Figure 6 (solid) and Table 2. These analyses were constrained by setting k_{21} and k_{10} to the values determined by the biexponential fits of the S_1 peaks, and $[S_2(0)]$ to the value determined by the S_0 Stokes data. This allowed for the determination of the following: (1) the cooling rate, k_{00}, for each vibrational mode, and (2) the enhancement factor, d, which measures the increase of anti-Stokes signal from S_0^{hot} relative to the room temperature S_0. Unconstrained fits, in which k_{10} was allowed to vary, converged to essentially the same value of k_{10} as the exponential fits, but with much larger errors in the parameters because of their interdependence. In Figure 6, it is apparent that the kinetic model and the exponential fits agree well with each other, although the initial incipient decrease in the C–CH_3 kinetics is not reproduced with the kinetic model. The expected decrease is too small compared with the measurement error to be statistically significant. The benefit of the kinetic

model is that we can definitively assign the mode-specific cooling rate associated with the observed anti-Stokes kinetics. The cooling time of the S_0 C=C peak is extremely fast, 0.7 ± 0.4 ps, and this band exhibits a very large enhancement factor of 171 ± 85. The S_0 C–C peak has a slower cooling time of 5.4 ± 0.9 ps and a smaller enhancement factor of 25 ± 3. The S_0 C–CH_3 peaks shows the slowest cooling time, 12.1 ± 2.5 ps, and the lowest enhancement factor, 12 ± 2.

The cooling rates in S_1 and S_0 can also be monitored by the time-dependent frequencies of the S_1 Stokes and the S_0 Stokes and anti-Stokes peaks. Figure 7 shows that the S_1 C=C peak blue shifts 10 cm^{-1} in <2 ps and that both the Stokes and anti-Stokes S_0 C–C peaks blue shift 3–4 cm^{-1} in <10 ps. The S_1 C=C frequency shift is fit with a 1.4 ps exponential rise time, consistent with the <2 ps S_1 cooling time determined using anti-Stokes intensity analysis (see below). The S_0 C–C frequency shifts with a ~5 ps time constant, consistent with the 5.4 ps C–C cooling time determined by the anti-Stokes intensity kinetics.

Discussion

Excited-State Spectra

Our S_1 Raman spectra of β-carotene are consistent with previous time-resolved Raman studies showing that vibrational bands of S_1 are highly shifted from the ground-state frequencies.[10,27–29] The 1157 cm^{-1} S_0 C=C peak splits into approximately 3 overlapping peaks at 1204, 1243, and 1282 cm^{-1} in S_1 and the 1523 cm^{-1} S_0 C–C peak splits into two peaks at ~1530 and ~1780 cm^{-1}. These frequency changes have been reproduced by the nonadiabatic vibronic coupling model of Zgierski et al.[30] Investigations of the high-frequency S_1 C–C peak in different solvents,[29] carotenoids,[31] and isotopomers[10] revealed that the S_1–S_0 frequency shift can be directly correlated with the extent of S_1–S_0 vibronic coupling. The 1781 cm^{-1} frequency of our S_1 C=C peak is consistent with previous observations in polarizable solvents.[29] However, our low-frequency 1543 cm^{-1} C=C peak can only be compared with previous experiments in a relatively nonpolarizable solvent (THF) in which the two S_1 C=C peaks were observed at 1530 and 1796 cm^{-1}.[10,32] The solvent dependence of the high-frequency C=C peak frequency has been attributed to a breakdown of C_{2h} symmetry in S_1 and the accompanied increase in S_1-S_2 vibronic coupling.[29] The upshift in our low-frequency C=C peak and the downshift of our high-frequency C=C peak relative to previous work by Koyama et al.[10,32] may be due to solvent dependent changes in the S_1–S_2 vibronic coupling. It is also possible that the lower C=C frequency observed in the previous work was affected by the spectral subtraction technique used, which is difficult because of the inherent spectral broadening of the ground-state spectrum at high powers and the close proximity of the S_0 and S_1 peaks around 1530 cm^{-1}.

Excited-State Vibrational Relaxation

One of our primary results is that there are no observable S_1 peaks in our high signal-to-noise anti-Stokes spectra. As summarized in Figure 8, this indicates that following fast internal conversion from S_2, molecules in S_1 equilibrate most of the excess photon energy (4600 cm^{-1}) as well as the energy of the $S_2 \rightarrow S_1$ internal conversion (5800 cm^{-1}) within 2 ps. As a result, there is no observable S_1 population in the high-frequency $v \geq 1$ vibrational levels. We estimate a maximum vibrationally excited population of <10% at 2 ps: On the basis of our limit-of-detection, we can place an upper limit on the anti-Stokes:Stokes intensity ratio of 15% for the C=C peak and 3% for the C–C peak at a time delay of 2 ps. Factoring in the ν_s^3 dependence of the Raman scattering, the population in $v \geq 1$ must be less than 10% and 2% of the total excited population within 2 ps after excitation for the C=C and C–C modes, respectively. Because it is unlikely that by 2 ps there would be more excitation in the higher frequency mode, we can place an upper bound of <2% on the S_1 vibrational excitation.

However, because under these resonance conditions the anti-Stokes scattering strength could be 5 times less than the Stokes scattering strength, a more conservative upper bound of <10% excitation is suggested. These results contrast with the conclusions of Yoshizawa et al.[15] on β-carotene and Zhang et al.[16] on lycopene who both hypothesized that relaxation in S_1 proceeds normally until the molecule is trapped in the $v = 1$ C–C vibrational state. If this were the case, then we would expect the percentage of vibrationally excited molecules in S_1 to be nearly 100% at and beyond 2 ps. A vibrationally excited population of this magnitude would almost certainly produce a large anti-Stokes signal, which we clearly do not observe. It is likely that the 0.6 ps relaxation rate observed by Yoshizawa et al. is reporting on the completion of the IVR process in S_1, rather than an incomplete relaxation to $v = 1$.[16] This fast IVR process, which has been observed in several other studies,[4,17] is much faster than could be detected with the 2–3 ps time resolution of Zhang et al.[15]

Excited-State Lifetime

The 12.6 ps S_1 lifetime determined here is slightly longer than those determined previously for β-carotene in aromatic solvents by transient absorption (8.4 ± 0.6, 10 ± 2, and 8.8 ± 0.2 ps).[16,33,34] This difference is most likely due to the fact that our experiment was performed at ~0–10 °C, whereas previous experiments were all performed at room temperature. Decreasing the sample temperature can as much as double the internal conversion time constant for carotenoids.[11] We can eliminate the possibility that our measured lifetimes are systematically increased as a result of interference with ground-state cooling features by noting the agreement of the S_1 lifetime measured by the 1781 cm^{-1} C=C peak with the average of the other four Stokes decay times. If there was a contribution from slow ground-state cooling process, we would expect the kinetics of the S_1 peaks at 1230 and 1543 cm^{-1} to be significantly longer than the kinetics of the 1781 cm^{-1} peak. However, since all of these decay times are within one standard deviation of each other, we conclude that ground-state cooling has a negligible affect on the measured lifetimes.

Ground-State Vibrational Relaxation

Analysis of the anti-Stokes kinetics is complicated by the slow rate of internal conversion between S_1 and S_0. Because IC necessarily occurs before the formation of hot S_0, any faster dynamics occurring within the ground-state manifold will be hidden. By examining the preexponential factors (α_i and β_i) in eq 5, it is apparent that with $k_{21} \gg k_{00} > k_{10}$ $(i.e.,\ \tau_{21} \ll \tau_{00} < \tau_{10})$, the kinetics of S_0^{hot} will be dominated by a rising term determined by k_{00}, the mode specific cooling rate, and a decaying term determined by k_{10}, the $S_1 \rightarrow S_0$ internal conversion rate. This is counterintuitive considering that schematically S_0^{hot} is formed via k_{10} and is removed via k_{00}. As a result, the exponential decays of the anti-Stokes kinetics (τ_0, Table 1) can be assigned to the $S_1 \rightarrow S_0$ internal conversion time and, as expected, they are all within one standard deviation of the 12.6 ps time constant determined in the Stokes kinetics. We assign the rising terms of the anti-Stokes kinetics (τ_1, Table 1) to the cooling times of these vibrational modes, however, these cooling times are better determined using the kinetic model (τ_{00}, Table 2). In general, it is apparent that the cooling times increase as the vibrational frequency decreases. As summarized in Figure 8, the 1523 cm^{-1} C=C relaxes in ~ 1 ps, the 1157 cm^{-1} C–C relaxes in ~5 ps, and the 1004 cm^{-1} C–CH_3 relaxes in ~12 ps. Our revised relaxation scheme becomes

$$S_0 \xrightarrow{h\nu} S_2 \xrightarrow{\tau_{21}=0.2\,ps} S_1 \xrightarrow{\tau_{10}=12.6\,ps} S_0^{hot} \xrightarrow{\tau_{00}=1-12\,ps} S_0 \quad (9)$$

The enhancement factor, d, determined by the anti-Stokes kinetic model is a measure of the increase in anti-Stokes scattering in S_0^{hot} relative to (cool) S_0. The enhancement arises from

either an increase in the resonance enhancement or from an increase in the vibrationally excited population. A large change in resonance enhancement can occur through two mechanisms, both of which are unlikely in this system. First, an increase in resonance enhancement of S_0^{hot} could occur if the S_0^{hot} scattering arose from a different vibrational transition than the S_0 scattering, which comes entirely from the $v = 0 \leftarrow 1$ transition. Our probe wavelength is approximately one vibrational quantum (~1400 cm^{-1}) below the S_2–S_0 electronic origin and is therefore very near the maximum in the $v = 0 \leftarrow 1$ anti-Stokes Raman excitation profile. Hence, at this wavelength we would expect to see only a decrease in relative scattering strength from molecules excited to vibrational states above $v = 1$.[35] Also, given that the rate of vibrational relaxation scales approximately linearly with vibrational quantum number,[36] it is unlikely that any high vibrational quantum number states would be present on the picosecond time-scale of our experiment. Second, changes in the resonance enhancement may occur with increasing temperature, even if the anti-Stokes scattering is generated from the $v = 0 \leftarrow 1$ transition. This would occur if there existed low-frequency modes that were strongly coupled to the resonant electronic transition; however, β-carotene has no strongly displaced low-frequency modes and, hence, should be relatively insensitive to this thermal multi-mode quenching.[25] We therefore conclude that most of the anti-Stokes scattering generated after IC is due to the $v = 0 \leftarrow 1$ transition in each mode and that the enhancement factors can be attributed to an increase in population of the $v = 1$ state.

Based on this conclusion, we can use our measured enhancements to estimate the degree of vibrational excitation in S_0^{hot}. Table 3 compares the observed occupation numbers after IC with the thermal occupation numbers that we would expect for different energy partitioning models. The thermal occupation numbers of each vibration in S_0 at 10 °C are 0.00043, 0.0028, and 0.0061 for the C=C, C–C, and C–CH_3 modes, respectively. Multiplying these values by d determines the observed occupation numbers in S_0^{hot}, which are 0.074, 0.070, and 0.073, respectively. If the S_1–S_0 internal conversion energy (14 500 cm^{-1})[37] is thermally distributed among all 282 normal modes of the molecule, the temperature will increase to 468 K. At this temperature the thermal occupation numbers for the C=C, C–C, and C–CH_3 modes will be 0.0093, 0.029, and 0.046, respectively, which are 22, 10, and 8 times larger than at 283 K but much less than necessary to generate the observed enhancements of 171, 25, and 12. Alternatively, if we distribute the full photon energy (24 814 cm^{-1}) in a Boltzmann population in S_0, then the temperature increases to 568 K. This would give occupation numbers of 0.021, 0.053, and 0.079 and enhancement factors of 49, 19, and 13 for the C=C, C–C, and C–CH_3 modes, respectively. The observed enhancements of the C=C and C–C modes are much larger than we would expect for a fully thermalized molecule, but the enhancement of the C–CH_3 mode is very nearly what we would expect based on thermalization of the photon energy throughout the molecule. This indicates that the C=C and C–C modes are preferentially excited by the IC process, whereas the C–CH_3 mode has no more excitation than that dictated by thermalization.

Vibrational Cooling

Following IVR, the energy of internal conversion is dissipated to the surrounding solvent environment through vibrational cooling. Our spectra reveal no long-term increase in anti-Stokes signal from β-carotene, indicating that vibrational cooling must occur in less than 13 ps. If the cooling rate were slower than the rate of internal conversion then there would be a build-up of anti-Stokes signal at long times and the decay of the anti-Stokes signal would exhibit biexponential kinetics. The relaxation time of the C–CH_3 mode (12 ps) is consistent with the 5–15 ps cooling time observed in longer carotenoids[4] and with our condition that the cooling must occur in <13 ps, so it is quite likely that the cooling time of the C–CH_3 mode is equivalent to the overall rate of energy dissipation to the solvent.

Implications for the Mechanism of IC and Ground-State IVR

Our cooling times and enhancement factors are consistent with a model of β-carotene relaxation in which the C=C and C–C stretching modes are the dominant acceptor modes in the internal conversion process. Because the observed enhancements are much larger than those calculated for a fully thermalized molecule, we conclude that the anti-Stokes signal from the C=C and C–C modes arises from hot ground-state molecules that have not fully thermalized on the ground state surface and that these modes must have received preferential excitation during IC. The extremely large enhancement factor of the C–C mode and the modest enhancement of the C–C mode indicate that the C–C mode is the primary acceptor, with the C=C mode being a minor acceptor. In contrast, the similarity of the C–CH_3 mode enhancement to that expected in a thermalized molecule indicates that its anti-Stokes signal is generated after IVR has been completed but before a significant amount of the photon energy has been dissipated to the environment. The rapid appearance of increased anti-Stokes signal from the C–CH_3 indicates that this mode must be excited by relaxation of the C=C mode.

It has been well established that the C=C is the primary promoting mode for S_1–S_0 internal conversion.[10,11,38] However, the accepting modes are not as well defined. Previous investigations of IC in β-carotene have been formulated in terms of the energy-gap law, which assumes that there is only one accepting mode that is weakly coupled to the electronic transition.[12] With this assumption, the insensitivity of the IC rate to deuteration,[11] and the sensitivity to ^{13}C substitution[10] has led to the conclusion that the C=C mode is the only acceptor. However, the assumption of a single accepting mode is not valid in β-carotene, which falls in Englman's strong-coupling limit[12] and has several modes of similar frequency and with very large displacements between S_1 and S_0 that may act as acceptor modes during IC.[37] By partitioning the IC energy into both the C=C and C–C modes, the Franck-Condon overlap between the relaxed S_1 state and the isoenergetic S_0 state can be dramatically increased. Also, because each of these modes would be similarly affected by ^{13}C-substitution, the isotope affect on the internal conversion rate would be the same as previously observed and predicted by the energy gap law.[10] The excitation of both the C=C and C–C modes by IC is also consistent with a twin-state model of the IC process, in which the S_1–S_0 conical intersection lies highly displaced from the S_0 equilibrium geometry along the bond-inversion coordinate.[13] Relaxation from the conical intersection to equilibrium would require simultaneous lengthening of C–C bonds and contraction of C=C bonds and so excitation of both of these normal modes would be expected.

Summary

Picosecond Stokes and anti-Stokes Raman spectra of photo-excited β-carotene have allowed us to directly observe relaxation processes in both the excited (S_1, $2A_g^-$) and ground (S_0, $1A_g^-$) states. The kinetics of the observed Stokes S_1 bands at 1781, 1543, and 1230 cm^{-1} as well as the kinetics of the S_0 Stokes spectral recovery, establish the $S_1 \rightarrow S_0$ IC time as 12.6 ps. The lack of any observable S_1 anti-Stokes signal indicates that β-carotene vibrationally relaxes via IVR within 2 ps in S_1, and that there is <10% residual vibrationally excited population by this time. Internal conversion between S_1 and S_0 partitions the IC energy between the C=C and C–C modes of the ground state. Although both of these modes act as acceptors, the magnitude of the anti-Stokes scattering indicates that the C=C mode is dominant. In the ground state, the mode-specific cooling rates are established by observing the growth and decay of the S_0 anti-Stokes signal. The 1523 cm^{-1} C–C mode relaxes in <1 ps, the 1157 cm^{-1} C=C mode in 5 ps, and the 1004 cm^{-1} C–CH_3 mode in 12 ps. The magnitude of the 1004 cm^{-1} mode anti-Stokes enhancement is consistent with a model of ground-state IVR in which the C–CH_3 mode is excited by IVR from the C=C mode. Finally, vibrational energy dissipation to the solvent must occur faster than the 12.6 ps $S_1 \rightarrow S_0$ IC because there is no long-lived enhancement of anti-Stokes scattering in S_0.

Acknowledgment

We thank Michael Tauber for many helpful discussions, Duohai Pan for performing the ab initio frequency calculations, and Kaiser Optical Systems, Inc. for the use of the notch filter. This work was supported by grants from the National Institutes of Health (EY02051) and the National Science Foundation (CHE-9801651).

References and Notes

1. Ritz T, Damjanovic A, Schulten K, Zhang JP, Koyama Y. Photosynth. Res 2000;66:125. [PubMed: 16228415]
2. SashimaTKoyamaYYamadaTHashimotoHRecently, the presence of a third short-lived excited state, the $1B_u^-$state, lying between the $2A_g^-$ and the $1B_u^+$ states has been proposed. J. Phys. Chem. B20001045011 Cerullo, G.; Lanzani, G.; Zavelani-Rossi, M.; De Silvestri, S. *Phys. Rev. B***2001**, *63*, 241 104)
3. Andersson PO, Bachilo SM, Chen RL, Gillbro T. J. Phys. Chem 1995;99:16 199.
4. Andersson PO, Gillbro T. J. Chem. Phys 1995;103:2509.
5. Shreve AP, Trautman JK, Owens TG, Albrecht AC. Chem. Phys. Lett 1991;178:89.
6. Zhang JP, Inaba T, Watanabe Y, Koyama Y. Chem. Phys. Lett 2000;332:351.
7. Kandori H, Sasabe H, Mimuro M. J. Am. Chem. Soc 1994;116:2671.
8. Akimoto S, Yamazaki I, Takaichi S, Mimuro M. Chem. Phys. Lett 1999;313:63.
9. Macpherson AN, Gillbro T. J. Phys. Chem. A 1998;102:5049.
10. Nagae H, Kuki M, Zhang JP, Sashima T, Mukai Y, Koyama Y. J. Phys. Chem. A 2000;104:4155.
11. Wasielewski MR, Johnson DG, Bradford EG, Kispert LD. J. Chem. Phys 1989;91:6691.
12. Englman R, Jortner J. Mol. Phys 1970;18:145.
13. Fuss W, Haas Y, Zilberg S. Chem. Phys 2000;259:273.
14. Garavelli M, Bernardi F, Olivucci M, Vreven T, Klein S, Celani P, Robb MA. Faraday Discuss 1998;110:51.
15. Zhang JP, Chen CH, Koyama Y, Nagae H. J. Phys. Chem. B 1998;102:1632.
16. Yoshizawa M, Aoki H, Hashimoto H. Phys. Rev. B 2001;63:180 301.
17. Cerullo G, Lanzani G, Zavelani-Rossi M, De Silvestri S. Phys. Rev. B 2001;63:241 104.
18. Polivka T, Zigmantas D, Frank HA, Bautista JA, Herek JL, Koyama Y, Fujii R, Sundstrom V. J. Phys. Chem. B 2001;105:1072.
19. Seilmeier, A.; Kaiser, W. Topics in Applied Physics. Ultrashort Laser Pulses: Generation and Applications. 2nd. Kaiser, W., editor. 60. Springer-Verlag; New York: 1993. p. 279
20. Hayashi H, Brack TL, Noguchi T, Tasumi M, Atkinson GH. J. Phys. Chem 1991;95:6797.
21. Okamoto H, Ogura M, Nakabayashi T, Tasumi M. Chem. Phys 1998;236:309.
22. Nakabayashi T, Okamoto H, Tasumi M. J. Phys. Chem. A 1997;101:3494.
23. Kim JE, McCamant DW, Zhu L, Mathies RA. J. Phys. Chem. B 2001;105:1240. [PubMed: 16755302]
24. Zhu L, Kim J, Mathies RA. J. Raman Spectrosc 1999;30:777.
25. Shreve AP, Mathies RA. J. Phys. Chem 1995;99:7285.
26. Saito S, Tasumi M. J. Raman Spectrosc 1983;14:310.
27. Hashimoto H, Koyama Y. Chem. Phys. Lett 1989;154:321.
28. Noguchi T, Kolaczkowski S, Arbour C, Aramaki S, Atkinson GH, Hayashi H, Tasumi M. Photochem. Photobiol 1989;50:603.
29. Noguchi T, Hayashi H, Tasumi M, Atkinson GH. J. Phys. Chem 1991;95:3167.
30. Orlandi G, Zerbetto F, Zgierski MZ. Chem. Rev 1991;91:867.
31. Noguchi T, Hayashi H, Tasumi M, Atkinson GH. Chem. Phys. Lett 1990;175:163.
32. Hashimoto H, Koyama Y. Chem. Phys. Lett 1989;163:251.
33. Wasielewski MR, Kispert LD. Chem. Phys. Lett 1986;128:238.
34. Bondarev SL, Bachilo SM, Dvornikov SS, Tikhomirov SA. J. Photochem. Photobiol. A 1989;46:315.
35. Okamoto H, Nakabayashi T, Tasumi M. J. Phys. Chem. A 1997;101:3488.
36. Kenkre VM, Tokmakoff A, Fayer MD. J. Chem. Phys 1994;101:10618.

37. Onaka K, Fujii R, Nagae H, Kuki M, Koyama Y, Watanabe Y. Chem. Phys. Lett 1999;315:75.

38. Negri F, Orlandi G, Zerbetto F, Zgierski MZ. J. Chem. Phys 1989;91:6215.

39. Frisch, MJ.; Trucks, GW.; Schlegel, HB.; Scuseria, GE.; Robb, MA.; Cheeseman, JR.; Zakrzewski, VG.; Montgomery, JA., Jr.; Stratmann, RE.; Burant, JC.; Dapprich, S.; Millam, JM.; Daniels, AD.; Kudin, KN.; Strain, MC.; Farkas, O.; Tomasi, J.; Barone, V.; Cossi, M.; Cammi, R.; Mennucci, B.; Pomelli, C.; Adamo, C.; Clifford, S.; Ochterski, J.; Petersson, GA.; Ayala, PY.; Cui, Q.; Morokuma, K.; Malick, DK.; Rabuck, AD.; Raghavachari, K.; Foresman, JB.; Cioslowski, J.; Ortiz, JV.; Stefanov, BB.; Liu, G.; Liashenko, A.; Piskorz, P.; Komaromi, I.; Gomperts, R.; Martin, RL.; Fox, DJ.; Keith, T.; Al-Laham, MA.; Peng, CY.; Nanayakkara, A.; Gonzalez, C.; Challacombe, M.; Gill, PMW.; Johnson, BG.; Chen, W.; Wong, MW.; Andres, JL.; Head-Gordon, M.; Replogle, ES.; Pople, JA. Gaussian 98, revision A.11.2. Gaussian, Inc.; Pittsburgh, PA: 2001.

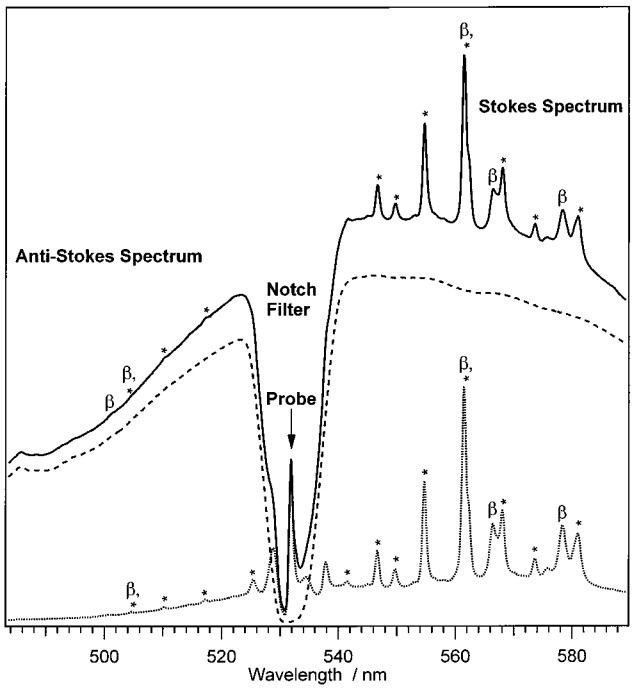

Figure 1.

Representative pump + probe (solid-line), pump-only (dashed line), and probe-only (dotted line) spectra of β-carotene. The pump + probe time delay is 1 ps. The dip in the middle of the spectrum is due to the notch filter, which removes scattered light within 5 nm of the probe wavelength (visible as the peak in the middle of the notch). Pump-induced fluorescence from S_2 spans the entire spectral window. Peaks labeled with an asterisk (*) are due to toluene. Peaks due to β-carotene are labeled "β".

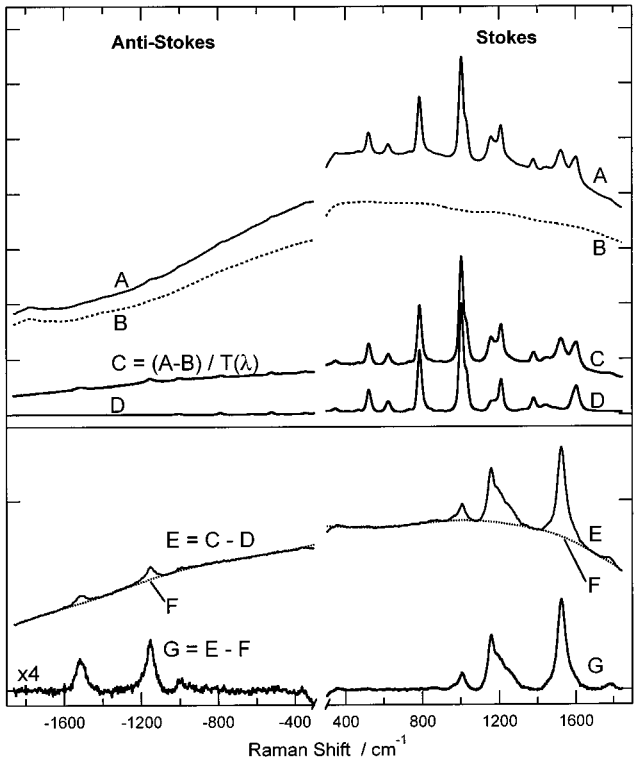

Figure 2.

Subtraction procedure used to produce time-resolved Raman spectra of β-carotene. The pump + probe spectrum (A) with Δt = 6 ps, pump-only spectrum (B, dashed), and toluene probe-only spectrum (D) were collected under the conditions described in the text. The pump induced fluorescence (B) is subtracted from the pump + probe spectrum (A) and corrected for β-carotene self-absorption by dividing by $T(\lambda)$, the β-carotene transmission spectrum. The toluene peaks in this spectrum (C) are removed by subtracting the toluene probe-only spectrum (D). The resultant spectrum (E) contains both β-carotene Raman scattering and residual fluorescence. The fluorescence background is fit (F, dotted) and subtracted to give the background free pump + probe Raman spectrum of β-carotene (G). The anti-Stokes region of spectrum G has been magnified ×4 for display.

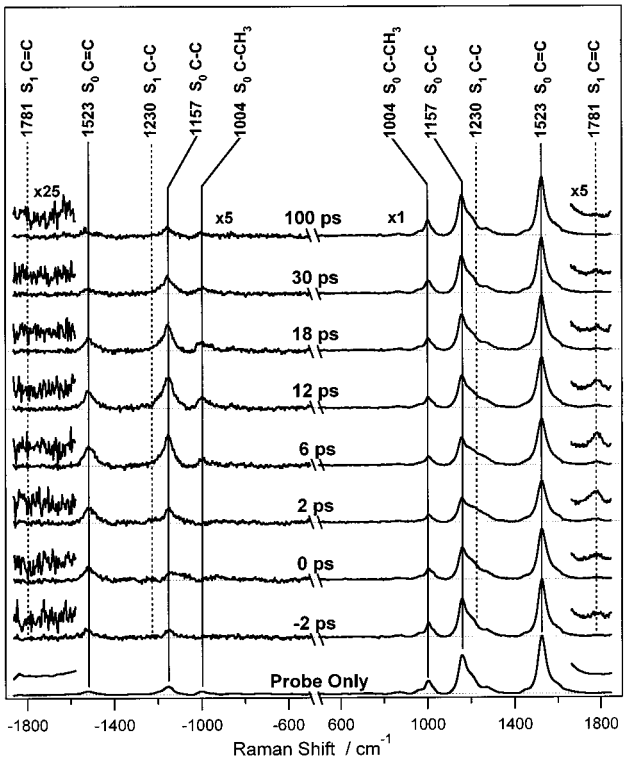

Figure 3.

Time-resolved pump + probe Raman spectra of β-carotene. Peaks from S_1 (marked by dashed vertical lines) are superimposed on peaks from S_0 (solid vertical lines). The anti-Stokes spectra (left side) are blown up ×5 for display. Note the decrease in intensity and subsequent recovery of the S_0 Stokes peaks and the large increase in S_0 anti-Stokes scattering caused by internal conversion from S_1 to S_0. The magnifications around ±1800 cm^{-1} reveal the appearance and decay of the S_1 C=C Stokes peak at 1781 cm^{-1} and the fact that no corresponding anti-Stokes peak is observed.

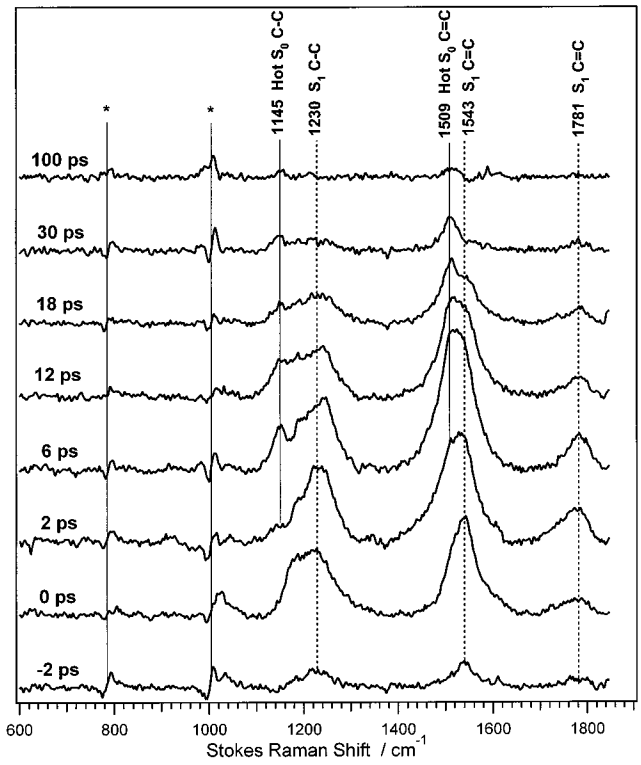

Figure 4.

Time-resolved Stokes difference spectra of β-carotene, produced by subtracting the probe-only S_0 spectrum from the time-resolved pump + probe spectra. Peaks attributed to S_1 are indicated with the dashed vertical lines. Residual scattering from the hot S_0 state is also observed, anharmonically red-shifted from the S_0 C–C and C–C bands. Features marked with an asterisk (*) are due to imperfect subtraction of toluene.

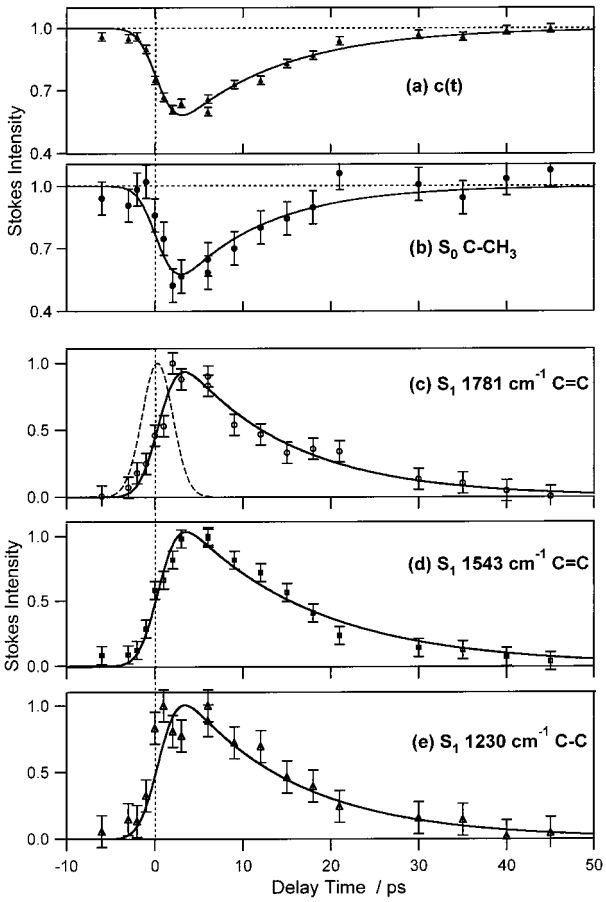

Figure 5.

Kinetics of the time-resolved Stokes spectra of β-carotene. The top two panels present the dynamics of S_0 population depletion and recovery. The subtraction coefficient, $c(t)$, was used to scale the probe-only spectrum in the generation of the Stokes difference spectra. The S_0 C–CH_3 intensity (b) is the integrated area of the methyl-rock peak at 1004 cm^{-1} in the pump + probe spectra. The bottom three panels present the dynamics of the S_1 state monitored by the Stokes difference spectra. The data points are the integrated areas of the S_1 C=C peak at 1781 cm^{-1} (c), the C=C band at 1543 cm^{-1} (d), and the C–C band at 1230 cm^{-1} (e). The 4.1 ps fwhm Gaussian instrumental response is shown as the dashed curve in (c). The solid curves are the fits of a convolution of the instrument response with the exponential molecular response described in eq 1. The fitting parameters are summarized in Table 1.

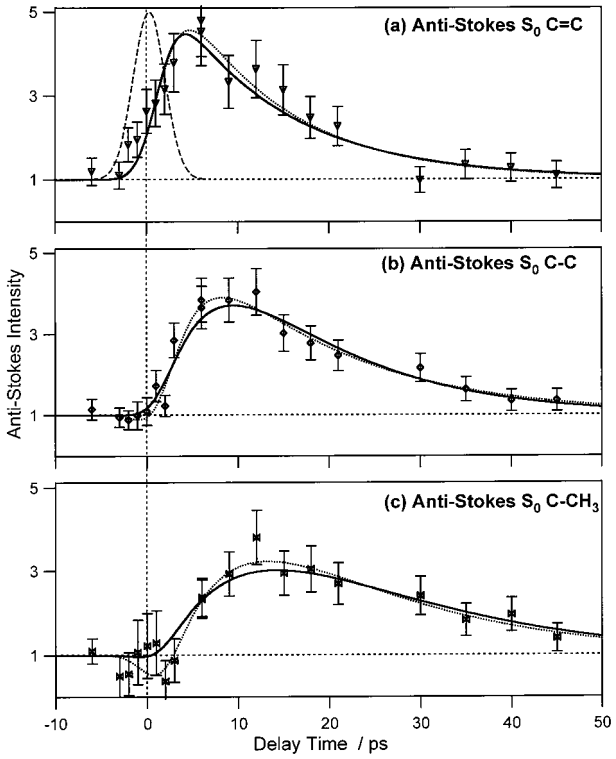

Figure 6.

Kinetics of the time-resolved anti-Stokes β-carotene spectra. Data points are the integrated areas of the anti-Stokes S_0 C=C peak at 1523 cm^{-1} (a), the S_0 C–C peak at 1157 cm^{-1} (b) and the S_0 C–CH_3 peak at 1004 cm^{-1} (c). The 4.1 ps fwhm Gaussian instrumental response is shown as the dashed curve in (a). The other curves are the best-fit convolutions of the instrument response with either a biexponential (eq 1, dotted) or kinetic (eq 8, solid) model of the molecular response. Values of the best fit parameters are summarized in Tables 1 and 2. Each peak area has been normalized to its area in the probe-only spectrum.

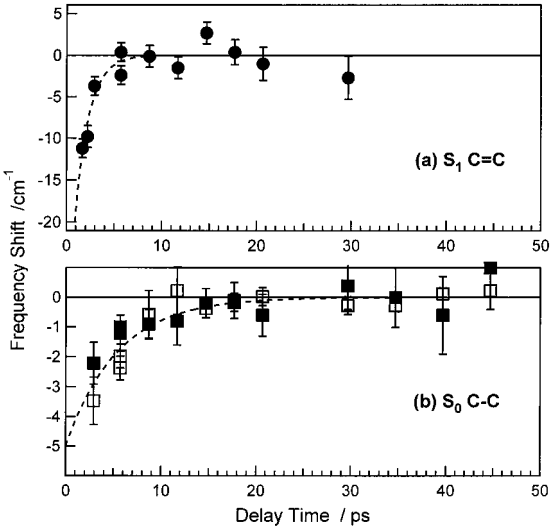

Figure 7.

Time-dependent frequency shifts of the S_1 C=C and S_0 C–C Raman peaks of β-carotene. (a) The frequency of the Stokes S_1 C=C mode relative to 1781 cm^{-1}. The dashed line is a 1.4 ps exponential decay. (b) The frequency shifts of the Stokes (open squares) and anti-Stokes (filled squares) S_0 C–C peaks relative to 1157 cm^{-1}. The dashed line is a 5.4 ps exponential decay, determined by the anti-Stokes C–C kinetics.

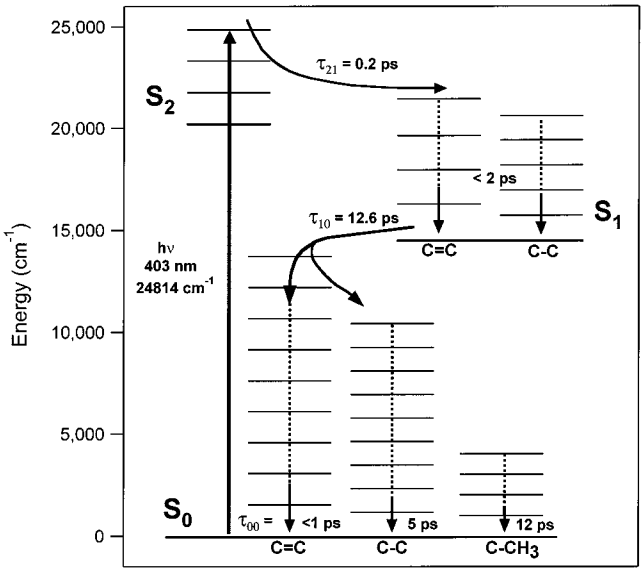

Figure 8.

Vibronic relaxation scheme of β-carotene. After excitation to S_2 ($1B_u^+$), the molecule relaxes in 0.2 ps to S_1 ($2A_g^-$). In S_1 IVR occurs very rapidly, such that the population of vibrational states with $v = 1$ is less than 10% within 2 ps. Internal conversion from S_1 to S_0 ($1A_g^-$) occurs with a 12.6 ps time constant. The C=C mode is the primary accepting mode of the IC process and relaxes in <1 ps through IVR. The C–C mode is excited directly by IC, as a minor accepting mode, and relaxes with a ~5 ps time constant. The C–CH_3 mode is excited by the IVR process and then relaxes with a 12 ps time constant, which is likely the molecular cooling rate.

TABLE 1

Exponential Analysis of β-Carotene Stokes and Anti-Stokes Intensities[a]

figure	component	A[b,c]	a_0	τ_0 (ps)	a_1	τ_1 (ps)
5_a	$c(t)$ Stokes subtraction coef.	−0.56 (0.02)	1	12.0 (0.7)	0	n.a.
5_b	S_0 Stokes C–CH_3 (1004 cm^{-1})	−0.59 (0.08)	1	10.2 (2.3)	0	n.a.
5_c	S_1 Stokes C–C (1781 cm^{-1})	1.27 (0.07)	1	12.6 (1.3)	−1	0.2[d]
5_d	S_1 Stokes C–C (1543 cm^{-1})	1.35 (0.06)	1	15.1 (1.2)	−1	0.2[d]
5_e	S_1 Stokes C–C (1230 cm^{-1})	1.42 (0.11)	1	13.2 (1.8)	−1	0.2[d]
6_a	S_0 anti-Stokes C–C (1523 cm^{-1})	5.9 (1.6)	1	11.7 (2.6)	−1	1.4 (0.7)
6_b	S_0 anti-Stokes C–C (1157 cm^{-1})	1	6.1 (2.2)	15.3 (3.7)	−8.3 (1.8)	3.1 (1.4)
6_c	S_0 anti-Stokes C–CH_3 (1004 cm^{-1})	1	8.8 (16)	16 (11)	−10.9 (15)	6.8 (5.5)

[a] Parameters were determined using eq 1 to model the data in Figures 5 and 6. The offset, B, was set to 1 in Figure 5a,b, 0 for 5c-e, and 1 for 6a–c.

[b] The $\Delta t = 0$ offset, Δt_0, was determined by initially allowing it to vary as a fitted parameter. The weighted average of these, 0.3 ± 0.1 ps, was chosen as the best overall value and fixed for these calculations.

[c] The amplitude, A, in 5a,b corresponds to the proportion of sample excited by the pump pulse. In 5c–e and 6a, A is a scaling factor without any molecular significance. In 6b,c, A is fixed at 1 to prevent redundancy when a_0 and a_1 are allowed to vary.

[d] The rise time, $\tau 1$, of the S_1 peaks was much faster than the time resolution of this experiment and could not be accurately determined. The value of 0.2 ps was chosen as described in the text.

TABLE 2

Kinetic Model Analysis of β-Carotene Anti-Stokes Intensities[a]

figure	component	τ_{21} (fixed) (ps)[b]	τ_{10} (fixed) (ps)[c]	τ_{00} (fit) (ps)	*d* (fit)[d]
6_a	S_0 C–C (1523 cm^{-1})	0.2	12.6	0.7 (0.4)	171 (85)
6_b	S_0 C–C (1157 cm^{-1})	0.2	12.6	5.4 (0.9)	25 (3)
6_c	S_0 C–CH_3 (1004 cm^{-1})	0.2	12.6	12.1 (2.5)	12 (2)

[a] Parameters were determined using eq 8 to model the data in Figure 6.

[b] The time constant for $S_2 \leftarrow S_1$ internal conversion, τ_{21}, was much faster than the time resolution of this experiment and could not, therefore, be experimentally determined. The value of 0.2 ps was chosen as described in the text.

[c] The $S_1 \leftarrow S_0$ time constant was calculated as the weighted mean of the decay times, τ_0, determined from the exponential fits to the Stokes kinetics (see Table 1).

[d] The enhancement factor, *d*, is an empirical measure of the increase in population in $v = 1$ of the hot S_0 state relative to the room-temperature S_0 state (see text).

Table 3

Observed and Calculated Thermal Occupation Numbers of β-Carotene

source	energy (cm^{-1})	*T* (K)	occupation number, ñ (ratio to 283 K value)[a]		
			C–C	C–C	C–CH_3
observed[b]	n.a.	850–550	0.074 (171)	0.070 (25)	0.073 (12)
sample temp.[c]	9388	283	0.00043 (1)	0.0028 (1)	0.0061 (1)
int. conv.[d]	14 500	468	0.0093 (22)	0.029 (10)	0.046 (8)
photon[d]	24 814	568	0.021 (49)	0.053 (19)	0.079 (13)

[a] Occupation numbers defined for a Boltzmann population at a given temperature as ñ = exp(-*hν*/*kT*). The energy stored at a given temperature is given by: $E_{\mathrm{vib}} = \sum_{i=1}^{282} h\nu_i / \left[\exp\left(h\nu_i / kT\right) - 1\right]$, where the vibrational frequencies of β-carotene were calculated by *Gaussian 98*[39] at the HF/3-21G level and scaled by 0.834. The scaling factor was chosen to place the calculated frequencies of the C–C, C–C, and C–CH_3 modes at the observed frequencies.

[b] Calculated by multiplying the sample temperature occupation numbers by the enhancement factor, *d*, determined spectroscopically. Note that the enhancement factors in parentheses are those determined in Figure 6 and shown in Table 2. The temperatures noted are the range of temperatures necessary to produce the calculated occupation numbers.

[c] Calculated assuming a Boltzmann distribution of vibrational excitation at 10 °C.

[d] The temperature was determined by adding either the S_1–S_0 internal-conversion energy (14 500 cm^{-1}) or the pump-photon energy (24 814 cm^{-1}) to the 9388 cm^{-1} of energy stored at 10 °C and distributing the net energy into a thermalized Boltzmann population of vibrations.